PERGAMON

International Journal of Multiphase Flow 27 (2001) 197–215

International Journal of Multiphase Flow

www.elsevier.com/locate/ijmulflow

Gravitational–centrifugal separation in an axisymmetric source–sink flow with a free surface

J. Mang[a,*], M. Ungarish[b], U. Schaflinger[a]

[a]*Institut für Strömungslehre und Wärmeübertragung, Graz University of Technology, Graz, Austria*
[b]*Department of Computer Science, Israel Institute of Technology, Haifa, Israel*

Received 2 October 1999; received in revised form 15 March 2000

Abstract

The inward source–sink flow of a dilute suspension with an upper free surface, in a cylinder with a horizontal solid bottom rotating about a vertical axis is analysed theoretically. The problem is made unique for the prescribed volume flux and outer radius by the requirement that the height of the interface at the outlet (drain) radius is minimal. A small Ekman number of the global flow and small Taylor and Reynolds numbers for the flow around the dispersed particles are assumed. The steady-state flow-field in the mixture bulk is described by an inviscid shallow water approximation. In addition, the influence of the horizontal shear layer at the bottom is incorporated by an Ekman-layer correlation. It turns out that in the investigated inward flow configuration, around the drain a domain may develop where the entire transport is performed by the Ekman layer. Theoretical predictions for the height of the fluid at the outer wall (position of the source) for various angular velocities are found to agree well with experimental results obtained earlier. The dispersed particles, assumed lighter than the fluid, separate from the main flow as a result of gravitational and centrifugal buoyancy. The numerical solution of the particle transport equation surprisingly shows that the concentration of the particles increases with the radius and, as expected, indicates the formation of a densely packed layer of particles on the top of the suspension.

Keywords: Centrifugal separation; Gravity separation; Source–sink flow; Rotating flow; Ekman layer

* Corresponding author.

0301-9322/01/$ - see front matter
PII: S0301-9322(00)00024-0

1. Introduction

The understanding and control of particle laden source–sink flows is very important in the analysis of geophysical flows and for the design of industrial processes, such as casting equipment. In metal casting, for example, special vessels are used for the gravity separation of light, solid impurities. Perturbations in the far field of the inflow lead to the creation of vorticity in many practical applications. The influx transports this vorticity to the drain of the vessel where it is usually concentrated as a strong local vortex, superimposing the sink flow. The resulting flow is commonly known as "bath-tub vortex". Rotational effects such as the formation of a viscous boundary region at the bottom of the vessel and the process of centrifugal separation are expected to influence the flow and separation of the suspension significantly, as indicated by Mang et al. (1998). Other related Source–sink studies of suspensions under centrifugal separation have been presented by Ungarish and Greenspan (1986) and Dahlkild and Amberg (1994). However, in the present problem, a combination of gravity and centrifugal effects, which has not been treated before to the best knowledge of the authors, is considered.

Some aspects of combined centrifugal–gravitational effects on the flow and separation of a suspension are investigated in this paper. A solution is presented for the flow-field and the particle concentration in a rotating source–sink flow of the type considered (for a pure fluid) by Whitehead and Porter (1977).

The first part of the study is concerned with the computation of the global flow-field, with separation disregarded. This is consistent with the practical assumption that the particle concentration is not large and hence does not significantly affect the driving forces of the velocity field. The analysis performed by Whitehead and Porter (1977) for a pure fluid serves as the starting point for the investigation of the basic flow inside the almost inviscid interior. The surface of the homogenous fluid is open to the atmosphere where a constant pressure p^*_{at} is assumed (Fig. 1). The analysis is limited to flows in which the free surface is sucked into the drain at the sink radius r^*_0. (Dimensional variables are marked by an upper asterisk.) This limiting condition, termed *condition of criticality*, is used as a boundary condition for the surface height at r^*_0. The present work extends Whitehead and Porter's approach by taking into account the viscous boundary layer at the bottom of the container by an Ekman layer

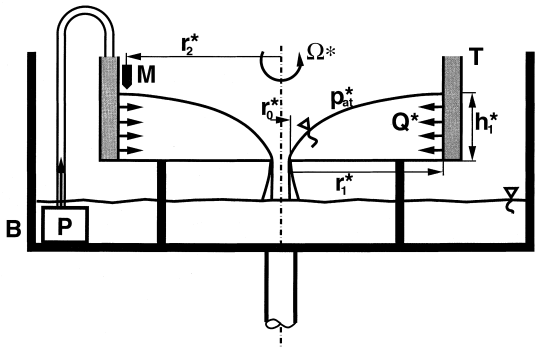

Fig. 1. Experimental apparatus.

approximation. The Ekman layer is expected to exert an important influence on the basic flow as the rate of rotation increases. It is assumed that

$$Ek = \frac{\nu^*}{\Omega^* h_1^{*2}} \ll 1 \tag{1}$$

where Ek is the Ekman number representing the ratio of viscous to Coriolis effects in the global motion; here ν^*, Ω^*, and h_1^* denote the kinematic viscosity of the pure fluid, the angular reference velocity, and the height of the free surface at r_1^* (Fig. 1), respectively. This definition is formally problematic because h_1^* is a part of the presently unknown solution. However, the physical meaning of Eq. (1) is, simply, that the layer of fluid is significantly thicker than the Ekman length $(\nu^*/\Omega^*)^{1/2}$, at least near the outer wall.

The behaviour of dispersed particles in the above-mentioned flow-field is considered in the second part of the investigation. Because the density of the particles is smaller than that of the embedding fluid, the suspension undergoes a process of separation caused by both gravitational and effective centrifugal buoyancy. The suspended particles are assumed to be spherical and of equal size and density. Furthermore, it is assumed that

$$Re_p = \frac{U^* a^*}{\nu^*} \ll 1, \qquad Ta_p = \frac{\Omega^* a^{*2}}{\nu^*} \ll 1, \tag{2}$$

with U^* as the Stokesian centrifugal settling velocity of a single spherical particle of radius a^* in a flow with the constant angular velocity Ω^* at the radius r_1^*. The Reynolds number, Re_p, represents the ratio of inertial and viscous forces acting on a dispersed particle. The Taylor number Ta_p represents the ratio of Coriolis and viscous forces on a dispersed particle. It follows from Eq. (2) that the hydrodynamic drag force on a suspended particle can be approximated by the Stokesian flow result.

2. The source–sink flow of the fluid

In the following, a theoretical model for the steady and critical withdrawal of a homogeneous fluid from a cylindrical tank rotating with a uniform angular velocity about its vertical axis, is developed. The problem is formulated in the cylindrical coordinate system (r, θ, z) that is co-rotating with the tank with angular velocity Ω^* about the vertical axis z. The velocity components are (u^*, v^*, w^*). The density of the liquid is denoted by ρ^*, the pressure by p^*, and the gravitational acceleration which acts in the $-z$ direction by g^*.

Axial symmetry is assumed. The model takes into account the effect of the Ekman layer on the (almost) inviscid interior flow. Inside the Ekman layer which is dominated by viscous shear, the inviscid flow inside the core is adjusted to the no-slip condition at the solid bottom wall of the container. At high rotation rates of the tank, a significant amount of the radial flux Q^* is sucked into the Ekman layer, thus considerably affecting the core flow.

Fig. 1 illustrates an experimental apparatus for the creation of such a flow, following Whitehead and Porter (1977). A basin B filled with water is mounted on a turntable which rotates about a vertical axis. A cylindrical tank T with sidewalls made of a porous material is

also mounted on this turntable. A pump P steadily feeds water from the basin into the sidewalls of the tank. Thus, an axisymmetric radial influx Q^* of height h_1^*, independent of the vertical coordinate, is produced at the radius r_1^*. The flux is eventually withdrawn through a circular hole of radius r_0^* in the bottom of the container. A micrometer probe M with an accuracy of ± 0.05 mm was used to measure the surface height h_2^* at a radius r_2^* (slightly smaller than the inflow radius r_1^*) for various values of Ω^* and Q^*.

Fig. 2 displays the flow when the action of the Ekman layer at the bottom of the container is included. The region of interest $r_0^* \leq r^* \leq r_1^*$ is divided into two domains of different flow patterns with a smooth transition between them. In domain a, the radial flux Q^* (negative in the radial direction) is partly transported through the core and partly in the Ekman layer, as follows

$$-Q^* = 2\pi r^* u^* h^* - \pi r^* v^* \left(v^*/\Omega^*\right)^{1/2}. \tag{3}$$

Although the flow is expected to be non-linear, the Ekman layer contribution to the volume-flux transport (the last term) was taken into account by a linear Ekman-layer correlation. This simplification, however, is expected to be a fair approximation; as a justification it is mentioned that the linear Ekman-layer correlation is a good approximation of both von Karman and Bödewadt non-linear boundary layers on a disk (see Greenspan, 1968). Due to angular momentum conservation, the azimuthal velocity v^* increases as the radius decreases (the details will be obtained later). Consequently, as the radius decreases, the radial Ekman layer volume transport increases, i.e., while moving inward the fluid is also sucked into the Ekman layer. According to Eq. (3) the increase of the second term is compensated by a decrease of the radial volume transport inside the core; at some radius r_E^* the radial velocity component of the core flow, u^*, vanishes. In the region of $r^* < r_E^*$ which is referred to as domain b the entire radial fluid transport goes through the Ekman layer. In order to distinguish flow regimes with both domain a and domain b from flow regimes in which no domain b is formed, the former will be referred to as "type a/b" and the latter as "type a".

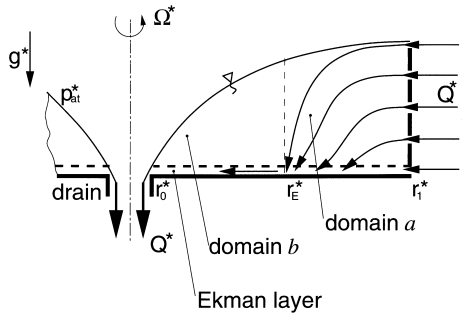

Fig. 2. Flow model with Ekman layer at the bottom. The flow-field is of type a when domain b does not appear, and of type a/b when both domains are present.

2.1. Mathematical formulation

To facilitate the comparison of the present theory with Whitehead and Porter's experimental findings, dimensional variables are used in the following section. The basic equations governing the interior flow are the equation of continuity and the Euler momentum equations. The "shallow water" simplifications are introduced, i.e., it is assumed that the axial velocity component is much smaller than the lateral (radial) component, and it is important to consider mainly the z-average motion in the core. The formal justification for this approach is that the height of the fluid layer is small as compared to its radius, $h^* \ll r_1^*$. Moreover, in the rotating case the velocity field in the core tends to be z-independent even in a thick layer of fluid. (This propensity, indicated by the Taylor–Proudman theorem in special limiting circumstances, remains valid even for large deviations from solid body rotation in axisymmetric inviscid steady-state bulks of fluid, because the small axial Ekman layer induced motion is unable to support a substantial $\partial p^*/\partial z^*$ beyond the hydrostatic field.) It is emphasised that the layer of fluid in the "shallow" core is much thicker than the viscous Ekman layer at the bottom.

Under these simplifications the momentum balance in the vertical direction is approximated by the hydrostatic balance which, on account of the free-surface condition $p^* = p_{\mathrm{at}}^* = \text{const.}$, yields

$$p^* = \rho^* g^* \left[h^*(r^*) - z^* \right] + p_{\mathrm{at}}^*. \tag{4}$$

Furthermore, in the following analysis the radial and azimuthal velocity components are represented by the corresponding z-averaged $u^*(r^*)$ and $v^*(r^*)$. The system of equations for the motion in the inviscid domain is therefore reduced to the following.

Radial momentum balance,

$$u^* \frac{\mathrm{d}u^*}{\mathrm{d}r^*} - \frac{v^{*^2}}{r^*} - 2\Omega^* v^* = -g^* \frac{\mathrm{d}h^*}{\mathrm{d}r^*} + \Omega^{*^2} r^*, \tag{5}$$

where the first term on the right-hand-side is the pressure gradient in accordance with Eq. (4); angular momentum balance,

$$u^* \left(\frac{\mathrm{d}v^*}{\mathrm{d}r^*} + \frac{v^*}{r^*} + 2\Omega^* \right) = 0; \tag{6}$$

and the kinematic condition which expresses the fact that fluid particles on the free surface $z^* = h^*(r^*)$ remain there,

$$u^* \frac{\mathrm{d}h^*}{\mathrm{d}r^*} = w^*(r^*, z^* = h^*). \tag{7}$$

In domain a, $u \neq 0$ and hence Eq. (6) yields a relation for v^* which can be easily integrated, subject to the boundary condition $v_1^* = 0$,

$$v^* = \Omega^* r_1^* \left(\frac{r_1^*}{r^*} - \frac{r^*}{r_1^*} \right), \quad r^* \geq r_{\mathrm{E}}^*. \tag{8}$$

In domain b, $u = 0$ in the core and hence Eq. (6) is trivially satisfied. In this case the angular velocity in the core is obtained from the Ekman-layer transport correlation (3) with $u = 0$. It readily follows that the azimuthal motion inside domain b is a potential vortex and that the Ekman layer below this core is non-divergent (see e.g. Greenspan, 1968):

$$u^* = 0, \quad v^* = \frac{Q^*}{\sqrt{\nu^*/\Omega^*}\pi}\frac{1}{r^*} = \frac{K^*}{r^*}, \quad w^*(z^* = 0+) = 0, \quad r^* \le r_E^*, \tag{9}$$

where $0+$ denotes the position of the "edge" of the Ekman layer.

The transition radius r_{E}^* is obtained by equating the expressions for the azimuthal velocities in domains a and b, as given by Eqs. (8) and (9), respectively,

$$r_{\mathrm{E}}^* = \sqrt{r_1^{*^2} - \frac{Q^*}{\pi\sqrt{\nu^*\Omega^*}}}. \tag{10}$$

The next task is to determine $h(r)$. Separate formulations are necessary for the $r \ge r_{\mathrm{E}}$ and $r \le r_{\mathrm{E}}$ domains, with matching at r_{E} when applicable.

For $r \ge r_{\mathrm{E}}$, substitution of Eq. (8) into Eq. (5), integration and some arrangement, yield a cubic equation for $h^*(r^*)$,

$$h^{*^3} - h^{*^2}H^*(r^*) + \frac{1}{2g^*}\left[-\frac{Q^*}{2\pi r^*} + \frac{\sqrt{\nu^*\Omega^*}}{2}\left(\frac{r_1^{*^2}}{r^*} - r^*\right)\right]^2 = 0, \quad r_{\mathrm{E}}^* \le r^* \le r_1^* \tag{11}$$

where

$$H^*(r^*) = h_B^* + \frac{u_B^{*^2}}{2g^*} + \frac{\Omega^{*^2} r_1^{*^4}}{2g^* r^{*^2}}\left(\frac{r^{*^2}}{r_B^{*^2}} - 1\right); \tag{12}$$

the subscript B denotes some reference position where boundary conditions are applied. For dimensionless considerations it is convenient to use the outer wall, with subscript 1, as the reference location, and introduce the scaling for the radius and heights as follows

$$r = \frac{r^*}{r_1^*} \quad , \quad h = \frac{h^*}{h_1^*} \quad , \quad H = \frac{H^*}{h_1^*}. \tag{13}$$

With these scalings the dimensionless form of Eq. (11) becomes

$$h^3 - \left[1 + Fr^2 + Fr_\Omega^2\left(1 - \frac{1}{r^2}\right)\right]h^2 + \left[-\frac{Fr}{r} + \frac{Ek^{\frac{1}{2}}Fr_\Omega}{2}\left(\frac{1}{r} - r\right)\right]^2 = 0, \tag{14}$$

where two Froude numbers appear,

$$Fr = \frac{u_1^*}{\sqrt{2g^*h_1^*}}, \qquad Fr_\Omega = \frac{\Omega^* r_1^*}{\sqrt{2g^*h_1^*}}, \tag{15}$$

which represent the ratio of the radial and azimuthal flow velocity to the propagation velocity

of a shallow water wave. This dimensionless formulation is, at this stage, less useful than could be anticipated because the dimensionless parameters Fr and Fr_Ω depend on the surface height h_1^* which is unknown a-priori in the present analysis. However, an a-posteriori evaluation of the parameters is instructive. In many cases of practical interest Fr (and also Fr_Ω) are small parameters. Therefore, the following analysis is restricted to $Fr < 1/\sqrt{2}$. The aforementioned condition refers to the subcritical regime of the shallow water theory (not to be confused with the condition of criticality which will be introduced in the next paragraph).

Only one of the the three roots of Eq. (11) is physically acceptable according to straightforward considerations given by Whitehead and Porter (1977).

For the domain $b, r \le r_E$, v^* given by Eq. (9) is substituted in Eq. (5), and subsequent integration yields

$$h^*(r^*) = h_0^* + \frac{1}{g^*}\left[2\Omega^* K^* \ln\frac{r^*}{r_0^*} - \frac{K^{*2}}{2}\left(\frac{1}{r^{*2}} - \frac{1}{r_0^{*2}}\right) + \frac{\Omega^{*2}}{2}\left(r^{*2} - r_0^{*2}\right)\right], \quad r_0^* \le r^* \le r_E^*. \tag{16}$$

Evidently, some boundary condition is needed for obtaining a unique result for h, in addition to the given values of r_0^*, r_1^*, Ω^* and, Q^*.

A *condition of criticality* is prescribed at the outlet and the flow is studied under this limiting condition. The condition of criticality for a flow-field of type a ($r_E^* \le r_0^*$) uses the fact that (14) predicts a vertical tangent for h at a certain $r = r(Fr, Fr_\Omega)$. In the regime of $Fr < 1/\sqrt{2}$, h has a positive slope. Considering also the equation of continuity $d(urh)/dr \approx 0$, it follows that the hydrostatic pressure gradient acts as a driving force, accelerating the flow as it propagates inward. This acceleration must be compensated by a decrease of h, which in turn causes a further acceleration of the flow until eventually a point is reached at which the slope of h becomes infinite and no further acceleration is possible. Tracing the solution $h(r)$ from the the outer wall r_1^* to smaller radii it becomes evident that the interface hits the bottom at the critical radius and the radial flow becomes impossible. The required boundary condition is obtained by identifying the sink radius r_0^* with this critical radius:

$$\frac{dh^*}{dr^*} = \infty \quad \text{at } r^* = r_0^*. \tag{17}$$

Returning to (11) with the condition (17) it follows that $h^*(r_0^*) = (2/3)H^*(r_0^*)$ and therefore an explicit result for $H^*(r_0^*)$ can be obtained. Consequently, using the known conditions at r_0^*, (12) can be reformulated as

$$H^*(r^*) = \frac{3}{2g^{*1/3}}\left[-\frac{Q^*}{2\pi r_0^*} + \frac{\sqrt{v^*\Omega^*}}{2}\left(\frac{r_1^{*2}}{r_0^*} - r_0^*\right)\right]^{2/3} + \frac{\Omega^{*2} r_1^{*4}}{2g^*}\left(\frac{1}{r_0^{*2}} - \frac{1}{r^{*2}}\right), \quad r_0^* \le r^* \le r_1^*. \tag{18}$$

A unique solution for $h^*(r^*)$ is now possible by Eqs. (11) and (18). This, however, is valid only when the domain b does not appear in the configuration.

For the flow of type a/b the radial volume transport near the sink, for any $r_0^* > 0$, can be performed by the Ekman layer without the need to increase the slope of the interface to infinity (the increase is now in the angular velocity). However, even in this case there is a clear-

cut limitation on the value of h_1^* for which a steady flow field can be reached with the sink positioned at r_0^*. This can be simply defined by identifying the sink radius with the radius at which no potential energy is left to push the fluid further inward. Thus,

$$h^*(r_0^*) = 0, \quad (r_0^* < r_E^*); \tag{19}$$

is the appropriate *criticality condition* for a flow of type *a*/*b*. This is, of course, an approximation ignoring the details of the expected thin and narrow viscous region where the flux from the thin Ekman layer is diverted into the sink.

The unique solution of $h^*(r^*)$ is again available. Using (16) subject to the condition in (19) yields readily $h^*(r^*)$ for $r_0^* \le r_E^*$. The value at r_E^* is then used to define $H^*(r^*)$, see (12) and recall that $u_E^* = 0$, and solve (11) for $r^* > r_E^*$.

In the following analysis the flow field is considered under the "critical" conditions imposed by either (17) or (19), according to the type of flow which appears near r_0^*. Whitehead and Porter (1977) noticed an interesting correlation for the variation of the height of the interface at a certain radius, say r_2^*, as a function of the angular velocity. They considered the inviscid case (with no Ekman layer) i.e., flow of type *a* in the entire radial domain. In this case the comparison of $H^*(r^*)$ given by Eqs. (12) and (18) with $\nu^* = 0$ in the non-rotating ($\Omega^* = 0$) and rotating circumstances, at the radii r_0^* and r_2^*, leads to the conclusion that the combination $h_2^* + u_2^{*2}/2g^*$ varies like the last term of (18) with $r^* = r_2^*$. Consequently, upon assuming $Fr \ll 1$ they obtained

$$h_2^* - h_{2_0}^* = (2\Omega^*)^2 / C^*, \quad \text{where } C^* = 8g^* r_0^{*2} r_2^{*2} / \left[r_1^{*4} \left(r_2^{*2} - r_0^{*2} \right) \right], \tag{20}$$

and $h_{2_0}^*$ is the height in the non-rotating case. Thus, the height of the interface at the radial position r_2^* is expected to increase like Ω^{*2}; moreover, the constant of proportionality depends only on geometrical properties of the configuration (not on the value of the throughput Q^*). To verify this prediction it is convenient to display experimental measurements of $(h_2^* - h_{2_0}^*)C^*$ versus $2\Omega^*$ in a log–log plot, expecting a straight line.

However, when the contribution of the viscous Ekman layer is taken into account, as in the present investigation, the behaviour of $(h_2^* - h_{2_0}^*)C^*$ versus $2\Omega^*$ becomes more complicated and less universal: now it depends also on the value of Q^*.

2.2. Results

Some results of the foregoing mathematical formulation are presented. The values of the parameters are the same as those used by Whitehead and Porter. The values of Q^*, the geometrical properties $r_0^* = 4.8$ cm, $r_1^* = 15$ cm, $r_2^* = 13.8$ cm, and the kinematic viscosity $\nu^* = 0.01$ cm^2 s^{-1} are as in Whitehead and Porter's experiment.

Fig. 3 shows a comparison on a log–log diagram of the theoretical predictions of the inviscid model (no Ekman layer) and of the present model for the reduced surface height at the probe radius vs. $2\Omega^*$. Both theories agree very well in the range $0.5\ \text{s}^{-1} < \Omega^* < 5\ \text{s}^{-1}$, which indicates that the Ekman layer effect is very small. At larger values of Ω^*, the present theory (full curve) predicts that the Ekman layer effects cause the height of the interface to decrease (as compared to the inviscid theory). This prediction is indeed in qualitative agreement with the experimental

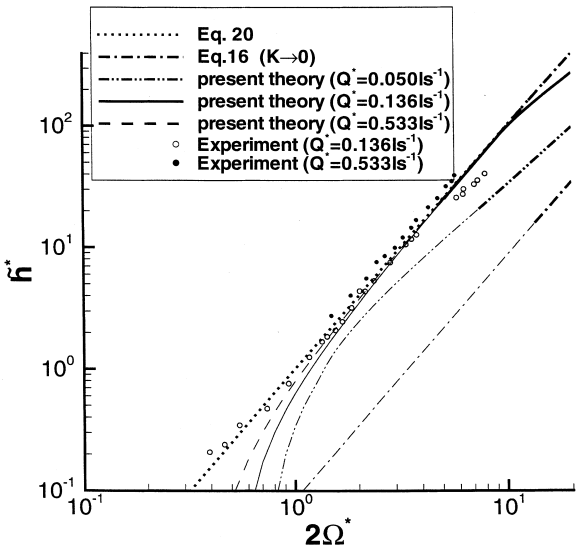

Fig. 3. Predictions for $\tilde{h}^*(2\Omega^*) = C^*(h_2^* - h_{2_0}^*)$ and experimental data (Whitehead and Porter, 1977. A micrometer probe with an accuracy of ± 0.05 mm was used to measure the surface height at radius r_2^* (slightly smaller than r_1^*) for various Ω^* and Q^*.

findings (open circles in Fig. 3). The curves corresponding to Eqs. (20) and (18) with $K \to 0$ are straight lines. They represent the asymptotic limits of large and small values of Q^* compared to $\pi\sqrt{\nu^*\Omega^*}r_1^{*2}$, because in the former case no domain b is formed and in the latter r_E^* tends to r_1^*. The relative importance of the Ekman layer increases as Q^* decreases. At very small values of Ω^*, the predictions of the inviscid and Ekman-influenced models disagree again. Here, however, both theories are expected to fail. In this range of parameters h_1^* corresponds to the thickness of the viscous Ekman layer and hence the assumption that an inviscid core exists, i.e., $\sqrt{Ek} \ll 1$, is violated. Indeed, the experimental results for $\Omega^* < 0.5\ \mathrm{s}^{-1}$ are clearly above the dotted curve (inviscid theory). Hence, the parts of the curves which do not satisfy $\sqrt{Ek} \ll 1$ (drawn as thin lines) are not covered by the available theories and should not be used for assessing the validity of our analysis.

Additional information about the pertinent flow fields is displayed in Figs. 4–7 and Table 1, for four different values of the angular velocity of the system Ω^* and $Q^* = 0.136\ \mathrm{l\ s}^{-1}$.

Fig. 4 shows that the dimensionless surface height increases as the Ekman number increases.

Table 1
Dimensionless parameters and flow characterizations for various Ω^*

Ω^* (s^{-1})	h_1^* (cm)	Fr	Fr_Ω	Ek	Flow type
0	0.41	1.26×10^{-1}	0	∞	a
2.5	6.45	1.99×10^{-3}	3.33×10^{-1}	9.61×10^{-5}	a
5	24.82	2.63×10^{-4}	3.40×10^{-1}	3.25×10^{-6}	a/b, $r_E = 0.37$
10	70.46	5.51×10^{-5}	4.03×10^{-1}	2.01×10^{-7}	a/b, $r_E = 0.63$

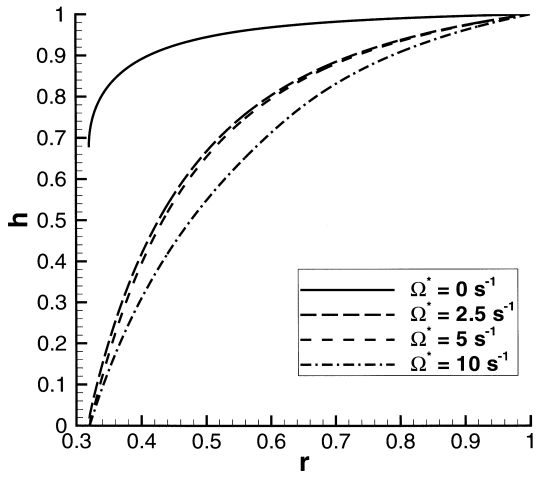

Fig. 4. Dimensionless surface height $h(r)$ for various Ω^* and $Q^* = 0.136\ \mathrm{l\ s^{-1}}$.

As rotation becomes less important (Ek increases), less fluid is pumped through the Ekman layer. Therefore, a higher amount of fluid has to be transported inside the core, leading to an increase of the slope of the surface at small radii.

Fig. 5 indicates that the dimensionless Ekman layer radial volume transport Q^*_{Ek}/Q^* decreases with Ek. Q^*_{Ek}/Q^* decreases with the radius and becomes 1 inside domain b. For the non-rotating case there is obviously no Ekman layer transport at all.

Fig. 6 shows the negative dimensionless radial component of the core velocity $-u^*/u^*_1$. Except for the region close to the drain, the negative radial velocity increases with Ek. In the case of a flow of type a/b ($\Omega^* = 5\ \mathrm{s^{-1}}$, $10\ \mathrm{s^{-1}}$) $-u$ increases with r inside domain a and vanishes as domain b is reached, whereas $-u$ decreases with r in flows of type a ($\Omega^* = 0\ \mathrm{s^{-1}}$,

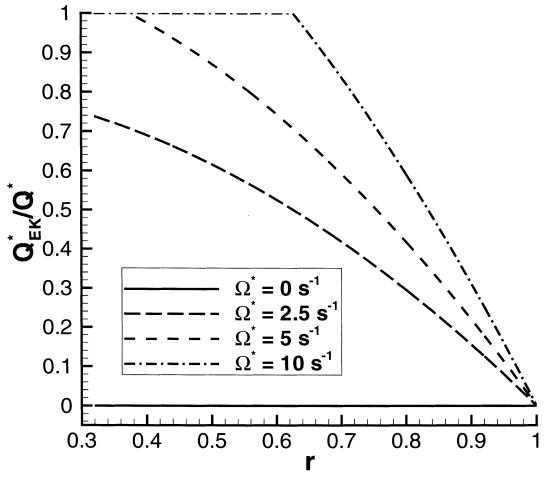

Fig. 5. Dimensionless radial volume transport $Q^*_{Ek}(r)/Q^*$ in the Ekman layer for various Ω^* and $Q^* = 0.136\ \mathrm{l\ s^{-1}}$.

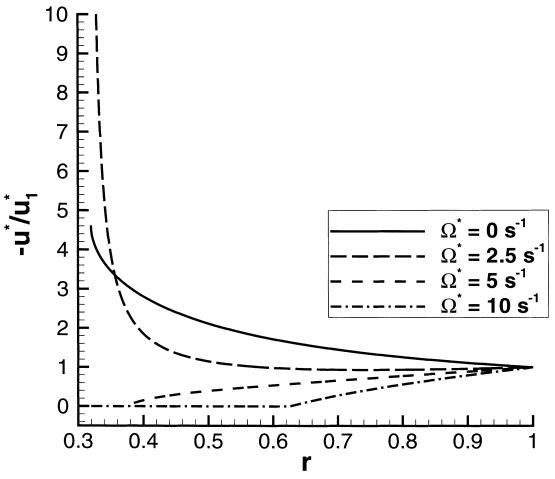

Fig. 6. Dimensionless radial core velocity component $-u^*(r)/u_1^*$ for various Ω^* and $Q^* = 0.136\,\mathrm{l\,s^{-1}}$.

2.5 s^{-1}). Near the drain, the curve corresponding to $\Omega^* = 5\ \mathrm{s}^{-1}$ reaches much higher values than the curve for the non-rotating flow, because h is much smaller in the former case than in the latter.

In Fig. 7 one can see that the dimensionless angular velocity $v^*/(r^*\Omega^*)$ increases as the radius decreases. Inside domain a, the dimensionless angular velocity does not depend on Ω^*, cf. Eq. (8). The deviation from solid body rotation (the effective Rossby number) is large. In flows of type a/b (dashed and dash-dotted curves), $v^*/(r^*\Omega^*)$ deviates for $r^* < r_E^*$ from the long-dashed curve representing flows of type a. The radius r_E^* at which the deviation begins increases with Ω^*.

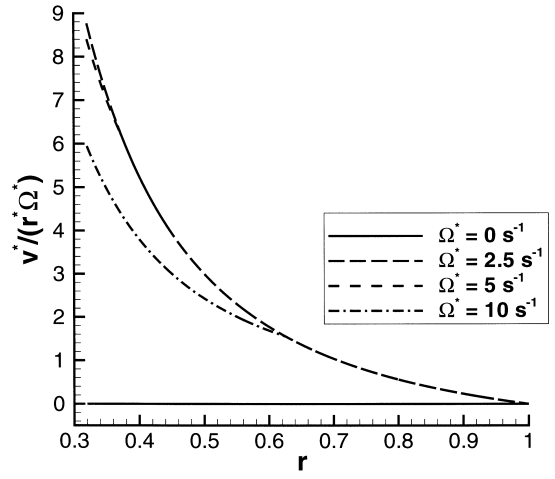

Fig. 7. Dimensionless angular velocity $v^*/(r^*\Omega^*)$ for various Ω^* and $Q^* = 0.136\,\mathrm{l\,s^{-1}}$.

3. Particle transport

An initially homogeneous suspension is considered in an axisymmetric, rotating, source–sink flow which incorporates the Ekman layer. Gravitational and centrifugal buoyancy cause the suspension to separate. The problem is formulated using the *mixture approach* (Ungarish, 1993) in which the suspension is regarded as a single flowing continuum with effective macroscopic properties. The aim of the following analysis is to find a solution for the volume fraction of the particle phase, α, as a function of space and time. To distinguish between the properties of the dispersed phase and those of the continuous phase, it is convenient to denote the former by the subscript "D" and the latter by the subscript "C". It is also important to distinguish between averaged mass velocity vectors, $\mathbf{v}^*$, and averaged volume flux vectors, $\mathbf{j}^*$. An important new variable is the relative velocity between the phases,

$$\mathbf{v}_R^* = \mathbf{v}_D^* - \mathbf{v}_C^*. \tag{21}$$

The particle transport is governed by the volume conservation of the dispersed phase which can be expressed (see e.g. Schaflinger, 1990) as

$$\frac{\partial \alpha}{\partial t^*} + \left[\mathbf{j}^* + (1-2\alpha)\mathbf{v}_R^*\right] \cdot \nabla\alpha = -\alpha(1-\alpha)\nabla \cdot \mathbf{v}_R^*, \tag{22}$$

where $\mathbf{j}^*$ is the volume flux of the mixture. When the relative density difference between the mixture and the pure fluid (the continuous phase) is small, the difference between $\mathbf{j}^*$ and $\mathbf{v}^*$ is also small. Restricting the present analysis to this case, the calculation of the velocity field can be decoupled from the solution of Eq. (22). In other words, the results obtained for $\mathbf{v}^*$ in the previous section are used to represent the flow-field of the mixture and the resulting behaviour of the dispersed particles is analysed according to Eq. (22), subject to proper initial and boundary conditions. Evidently, there is a strong relationship between $\alpha(\mathbf{r}^*, t^*)$ and the variable $\mathbf{v}_R^*$, and it will be shown below that this variable can also be directly correlated to the velocity field of the mixture.

3.1. Mathematical formulation

Dimensionless variables are defined by

$$\left\{r^*, h^*, z^*, u^*, v^*, w^*, \omega^*, t^*\right\} = \left\{r_1^* r, h_1^* h, h_1^* z, U^* u, \Omega^* r_1^* v, U^* w, \Omega^* \omega, \left(r_1^*/U^*\right)t\right\}, \tag{23}$$

with

$$U^* = \frac{2\varepsilon a^{*2}}{9\nu^*}\Omega^{*2} r_1^* \tag{24}$$

as the absolute value of the Stokesian centrifugal settling velocity of a single spherical particle at the radius r_1^* in a fluid rotating with constant angular velocity Ω^*. The velocity components, using Eqs. (3) and (8), are

$$\mathbf{j}_a^* = \mathbf{v}_a^* = \begin{pmatrix} -\dfrac{Q^*}{2\pi r^* h^*} + \dfrac{\sqrt{Ek}}{2} h_1^* \dfrac{\Omega^* r_1^*}{h^*} \left(\dfrac{r_1^*}{r^*} - \dfrac{r^*}{r_1^*} \right) \\ \Omega^* r_1^* \left(\dfrac{r_1^*}{r^*} - \dfrac{r^*}{r_1^*} \right) \\ w_a^* \end{pmatrix}, \tag{25}$$

where the subscript "a" stands for "domain a" and w_a^* denotes the vertical velocity component of the mixture flow. Considering (2), a simple relation for the relative interphase velocity $\mathbf{v}_{\mathrm{R}_a}^*$ is obtained from a balance between the local body force which comprises gravitational and centrifugal buoyancy, and the Stokesian drag on a single spherical particle calculated with the effective dynamic viscosity of the mixture μ_{eff}^*:

$$\mathbf{v}_{\mathrm{R}_a}^* = \frac{2\varepsilon a^{*2}}{9\nu^*} \frac{(1-\alpha)}{\mu(\alpha)} \begin{pmatrix} -\Omega^{*2} r^* \left[1 + \dfrac{r_1^*}{r^*} \left(\dfrac{r_1^*}{r^*} - \dfrac{r^*}{r_1^*} \right) \right]^2 \\ 0 \\ g^* \end{pmatrix}, \tag{26}$$

with

$$\varepsilon = 1 - \rho_{\mathrm{D}}^*/\rho_{\mathrm{C}}^* > 0.$$

The effective dynamic viscosity of the mixture is given as

$$\mu_{\mathrm{eff}}^* = \mu(\alpha)\mu_0^* = (1-\alpha)^{-3.1}\mu_0^*, \tag{27}$$

where μ_0^* denotes the dynamic viscosity of the pure fluid. (The correlation for $\mu(\alpha)$ introduced here is commonly used; it can be replaced with other similar correlations without any qualitative modification of the results.)

An expression for the volume flux vector $\mathbf{j}_b^*$ of the mixture inside domain b analogous to Eq. (25), is obtained, using (9):

$$\mathbf{j}_b^* = \mathbf{v}_b^* = \begin{pmatrix} 0 \\ K^*/r^* \\ w_b^* \end{pmatrix}, \tag{28}$$

with w_b^* denoting the vertical velocity component of the mixture flow in domain b. The vector of the relative interphase velocity in domain b is given by

$$\mathbf{v}_{R_b}^* = \frac{2\varepsilon a^{*2}}{9\nu^*} \frac{(1-\alpha)}{\mu(\alpha)} \begin{pmatrix} -r^* \left(\Omega^* + \dfrac{K^*}{r^{*2}} \right)^2 \\ 0 \\ g^* \end{pmatrix}. \tag{29}$$

The vertical velocity components of the mixture flow in both domain a and b are still

unknown. They have to be derived by integrating the continuity equation in the respective domains. At $z = 0$, the boundary conditions for the integration are given by the Ekman layer suction and at $z = h(r)$ they are given by the kinematic relation (7). As mentioned before, the Ekman layer is non-divergent inside domain b. Integration of the continuity equation yields the general result

$$w = c_1(r)z + c_2(r). \tag{30}$$

With the boundary conditions

$$w_a = -\frac{\sqrt{\nu^*\Omega^*}}{U^*} \quad \text{at } z = 0,$$

$$w_a = \frac{h_1^*}{r_1^*}u\frac{\mathrm{d}h}{\mathrm{d}r} \quad \text{at } z = h \tag{31}$$

the dimensionless vertical velocity component of the mixture in domain a becomes

$$w_a = A\left\{\left[\left(\frac{B}{2}\left(\frac{1}{r} - r\right) - \frac{Fr}{\gamma}\frac{1}{r}\right)\frac{1}{h^2}\frac{\mathrm{d}h}{\mathrm{d}r} + B\frac{1}{h}\right]z - B\right\}, \tag{32}$$

with the Froude number γ as

$$\gamma = \frac{U^*}{\sqrt{2g^*h_1^*}}, \tag{33}$$

and $A = h_1^*/r_1^*$ and $B = \sqrt{Ek}Fr_\Omega/\gamma$.

With the boundary conditions

$$w_b = 0 \quad \text{at } z = 0,$$

$$w_b = 0 \quad \text{at } z = h, \tag{34}$$

which follow from Eq. (9), the vertical velocity component of the mixture inside domain b becomes

$$w_b = 0. \tag{35}$$

Substituting $\mathbf{j}_a^*$, $\mathbf{v}_{\mathrm{R}_a}^*$ and $\mathbf{j}_b^*$, and $\mathbf{v}_{\mathrm{R}_b}^*$ into (22) eventually yields a quasi-linear, hyperbolic, differential equation of first order for $\alpha(r, z, t)$. This equation has to be formulated separately for domains a and b. Non-dimensionalising the equations with the scaling parameters given in Eq. (23) yields

$$\frac{\partial\alpha}{\partial t} + \left[-\frac{Fr}{\gamma}\frac{1}{rh} - \frac{1}{r^3}\frac{\partial\varphi(\alpha)}{\partial\alpha} + \frac{B}{2}\frac{1}{h}\left(\frac{1}{r} - r\right)\right]\frac{\partial\alpha}{\partial r} + \left[\frac{1}{A}w_a + C\frac{\partial\varphi(\alpha)}{\partial\alpha}\right]\frac{\partial\alpha}{\partial z} = -2\varphi(\alpha)\frac{1}{r^4} \tag{36}$$

for the particle concentration inside domain a, and

$$\frac{\partial\alpha}{\partial t} - r\left(1+\frac{\mathrm{D}}{r^2}\right)^2 \frac{\partial\varphi(\alpha)}{\partial\alpha}\frac{\partial\alpha}{\partial r} + \mathrm{C}\frac{\partial\varphi(\alpha)}{\partial\alpha}\frac{\partial\alpha}{\partial z} = 2\varphi(\alpha)\left[1-\frac{1}{r^4}\left(1+\mathrm{C}^2\right)\right] \tag{37}$$

for the particle concentration in domain b. In Eqs. (36) and (37) h follows from (11) and (16), respectively, and

$$\varphi(\alpha) = \alpha(1-\alpha)^{5.1}. \tag{38}$$

where γ, A and B are as defined above and the additional dimensionless parameters appearing in these equations are $C = 1/(2Fr_\Omega^2)/A^2$ and $D = K^*/(\Omega^* r_1^{*2}) = 2FrFr_\Omega/\sqrt{Ek}$, where K is defined in Eq. (9). The initial conditions and boundary conditions for Eqs. (36) and (37) are

$$\alpha = \alpha_0 \ \forall r_0 \le r \le 1 \quad \text{and} \quad 0 \le z \le h \text{ at } t = 0, \tag{39}$$

and

$$\alpha = \alpha_0 \quad \forall t > 0, \text{ at } r = 1,$$

$$\alpha = 0 \quad \forall t > 0, \text{ at } r_0 \le r < 1 \text{ and } z = 0.$$

They represent homogeneous particle concentration within the whole domain at $t = 0$, and inflow with the initial concentration, respectively. The boundary condition at $z = 0$ reflects the assumption that the suction velocity of the Ekman layer is smaller than the velocity of gravity settling. This requires the condition $\gamma/(Ek^{1/2}Fr_\Omega^3) > 1$.

Eqs. (36) and (37) were solved by the method of characteristics. A fourth order Runge–Kutta solver was used for integration. The particle concentration $\alpha(r, z, t)$ tends to a steady state. Fig. 8 shows a sketch of the particle distribution at a particular moment within the transient state. A domain of pure fluid (domain 1) develops at the bottom of the container. A kinematic shock separates it from the mixture region (domains 2 and 3). This shock is associated with the intersection of characteristic lines released with $\alpha = \alpha_0$ at $t = 0$ and characteristics released at the bottom boundary with $\alpha = 0$ at $t > 0$. It represents the locus of the "last" particles, i.e., the locus of particles which were initially in touch with the bottom boundary. The shape and position of the shock front, which initially coincides with the boundary, can be calculated by

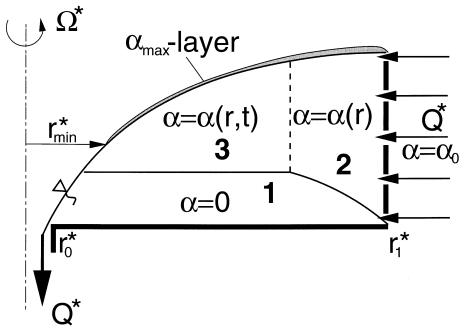

Fig. 8. Regions of different α during transitional state.

$$\frac{\partial \Sigma}{\partial t} + \mathbf{v}_{\mathrm{D}}^{+} \cdot \nabla \Sigma = 0, \tag{40}$$

with $\Sigma(\mathbf{r}, t) = 0$ as the implicit equation of the locus of the shock and $\mathbf{v}_{\mathrm{D}}^{+}$ as the local velocity of the dispersed phase on the mixture side of the shock. In the dilute limit, however, the difference between the velocity of the shock front and the propagation velocities of characteristics associated with $\alpha = \alpha_0$ and $\alpha = 0$, respectively, vanishes.

The mixture domain can be subdivided into a region in which α has already reached its steady state (domain 2) and a region in which α is still time dependent (domain 3), as indicated in Fig. 8. In the steady state region, α is determined by the characteristics emanating from the sidewall. In the transient region, α is still determined by characteristics released in the interior with the information of the initial condition. Because the effective centrifugal acceleration causes the radial velocity of characteristics to decrease with r (u_{R} decreases with r and α increases with r; see Fig. 11), characteristics cannot "catch" and intersect other characteristics released at smaller radii. Thus, the transition between the two regions (marked by the dashed line) is continuous.

It follows from Eqs. (36) and (37) that α is independent of z along characteristic lines. Because the initial conditions and boundary conditions at the sidewall are also independent of z, the particle concentration in the whole region of interest is known, once α along the mixture side of the kinematic shock has been determined. The particle concentration on the mixture side of the kinematic shock is obtained from the aforementioned characteristics.

When the transient domain has shrunk to zero, α has reached a steady state within the entire region of interest (Fig. 9). Note that the present approach does not take into account what happens to the particles when they reach the free surface. It is assumed here that a stationary layer of densely packed particles (referred to as $\alpha_{\max}$-layer in the following) develops above the mixture domain, as sketched in Fig. 9. A detailed analysis of the motion and stability of the expected $\alpha_{\max}$-layer is beyond the scope of the present investigation. However, a rough estimate for a minimal radius $r_{\min}$ confining the $\alpha_{\max}$-layer is obtained from a balance between gravity and the centrifugal force acting on a particle at the surface:

$$\frac{\mathrm{d}h}{\mathrm{d}r} = 2Fr_{\Omega}\omega^2 r, \quad \text{at} \quad r = r_{\min}. \tag{41}$$

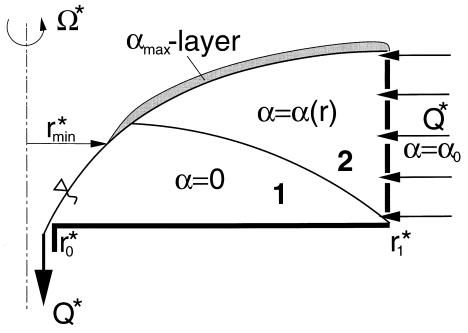

Fig. 9. Regions of different α in steady state.

Figs. 10 and 11 show the position $z(r, t)$ of the kinematic shock and the distribution of $\alpha(r, t)$ on the mixture side of the shock at various times t, for $Q^* = 0.136$ l s^{-1}, $r_0^* = 4.8$ cm, $r_1^* = 15$ cm and $\Omega^* = 5$ s^{-1} ($r_E = 0.37$). In Fig. 10 the curve with the label "h" represents the surface and the curves with the labels "t" and "steady state" represent the kinematic shock. The shock moves upward until it eventually reaches its steady state position.

The corresponding normalised values of α along the shock are given in Fig. 11. The concentration profiles show interestingly that the particle concentration increases with the radius. Since a suspension of light particles is considered, the observed behaviour is unexpected. In a rotating suspension of light particles one would rather expect α to increase as the radius decreases. The reason for this unusual behaviour is that here the effective centrifugal acceleration, which is controlled by the local swirl of the fluid, is different from the classical $\Omega^{*2} r^*$. Consequently, more particles are withdrawn to the α_{max}-layer than can be replaced by the influx with the initial particle concentration. This behaviour can be anticipated considering the RHS of (22). For a suspension of light particles in solid body rotation $\mathbf{v}_R \propto -Cr\hat{\boldsymbol{r}}$, whereas, in the present case $\mathbf{v}_{R_a} \propto -(C/r)\hat{\boldsymbol{r}}$, where C is a positive constant. Consequently $\nabla \cdot \mathbf{v}_R$ is negative in the former case and positive in the latter case.

As Ω^* increases, radial separation intensifies, thus leading to a decrease of the pure fluid region. The boundary between domains a and b appears as a point of non-smoothness in the curves for the particle concentration (Fig. 11). In Fig. 11 at $t = 10^{-3}$ a second kink can be seen at a smaller radius. The part of the curve on the left of this kink is given by characteristics which were released within domain b. The right part is determined by characteristics released in domain a. The vertical motion of the mixture caused by the Ekman layer suction and the adjustment of the surface is negligible within the investigated range of parameters compared to the vertical settling velocity of the particles. Thus, the position of the shock indicates only a very weak dependence on the radius.

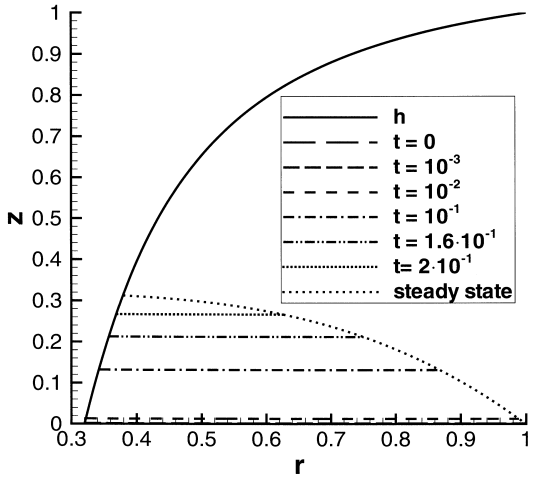

Fig. 10. Position of kinematic shock $z = z(r, t)$ for $\alpha_0 = 10^{-3}$, $Fr = 2.63 \times 10^{-4}$, $Fr_\Omega = 3.40 \times 10^{-1}$, $Ek = 3.25 \times 10^{-6}$, $\gamma = 2.27 \times 10^{-3}$, $A = 1.65$; $B = 0.27$, $C = 1.58$, $D = 0.86$.

4. Concluding remarks

The velocity and volume fraction fields in a steady axisymmetric source–sink flow of a rotating suspension in the configuration displayed in Fig. 1 were analysed theoretically. The flow is "critical" in the sense that the height of the interface at the sink radius is minimal. The influence of the viscous layer at the bottom was incorporated by a linear Ekman-layer correlation. It was found that for non-small rates of rotation, the Ekman layer exerts a significant influence on the almost inviscid interior flow; moreover, at small radii the entire volume transport is performed in the Ekman layer. The suction of the Ekman layer causes a reduction of the height of the fluid (as compared to predictions of an earlier analysis by Whitehead and Porter (1977), which neglects all viscous effects). This result is in good agreement with the experimental observations of Whitehead and Porter (1977).

The suspended lighter particles perform a complex motion since they are both convected by the fluid motion as well as separated by centrifugal and gravitational buoyancy effects. The transport equation for the particles was solved by the method of characteristics. It was found that the volume fraction of the particle phase in the suspension domain has a steady state in which $\alpha = \alpha(r)$. At the bottom of the container a region of pure fluid is formed which is separated by a kinematic shock from the mixture domain. As Ω^* decreases, the size of the pure fluid region decreases. The effective centrifugal acceleration, which differs from r, leads to the unexpected result of an increase of α with r.

This study is based on several simplifying assumptions, such as the shallow-water approximation, the Ekman-layer transport correlation and the decoupling between the fluid and the particle motion. The combination of all these assumptions yields formally quite strong restrictions on the practical parameter range of confident and accurate applicability. Nevertheless, the physical insight gained is expected to be useful. Further studies should assess the accuracy of the results by a more rigorous solution, requiring a large computational effort, or by new experiments. Experiments are also expected to throw light on the last stage of

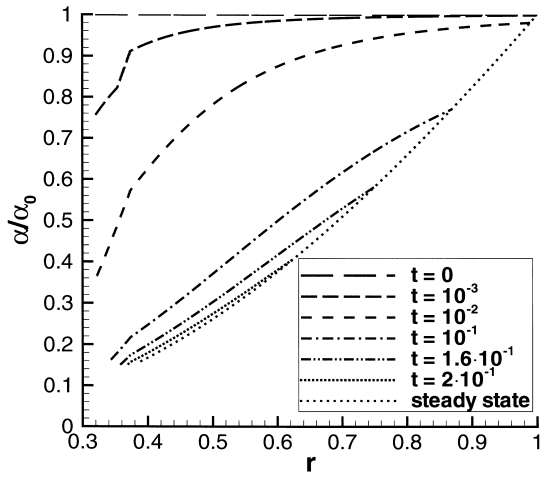

Fig. 11. $\alpha(r, t)/\alpha_0$ along kinematic shock.

motion of the dispersed particles (recall that the particles that separate from the suspensions are transported to the open interface, but their motion afterwards could not be pursued by the present investigation).

Acknowledgements

The authors would like to thank the Program of Scientific–Technological Cooperation Austria–Israel and the Fund for the Promotion of Research at the Technion University, Israel, for their financial support of this project.

References

Dahlkild, A., Amberg, G., 1994. Rotating axial flow of a continuously separating mixture. Journal of Fluid Mechanics 226, 319–346.

Greenspan, H.P., 1968. The Theory of Rotating Fluids. Cambridge University Press, London, New York (Reprinted by Breukelen Press, Brookline, 1990.).

Mang, J., Minkov, E., Schaflinger, U., Ungarish, M., 1998. Particle entrainment in a bounded rotating flow with a drain. ASME Journal of Fluids Engineering 120, 676–679.

Schaflinger, U., 1990. Centrifugal separation of a mixture. Fluid Dynamics Research 6, 213–224.

Ungarish, M., 1993. Hydrodynamics of Suspensions. Springer, Berlin.

Ungarish, M., Greenspan, H.P., 1986. On the radial filling of a rotating cylinder with a mixture. Journal of Fluid Mechanics 162, 117–128.

Whitehead, J.A., Porter, D.L., 1977. Axisymmetric critical withdrawal of a rotating fluid. Dynamics of Atmospheres and Oceans 2, 1–18.